Ultrasonics 91 (2019) 92–102

Contents lists available at ScienceDirect

Ultrasonics

journal homepage: www.elsevier.com/locate/ultras

The application of ultrasonic waves and envelope energies in a closed chamber based on an air/methane mixture

Kwonse Kim[a], Dooseuk Choi[b], Seokyeon Im[c,*]

[a] Green Car Technology Institute, Kongju National University, 1223-24, Cheonan-daero, Seobuk-gu, Cheonan-si, Chungnam 31080, Republic of Korea
[b] Division of Mechanical & Automotive Engineering, Kongju National University, 1223-24, Cheonan-daero, Seobuk-gu, Cheonan-si, Chungnam 31080, Republic of Korea
[c] Department of Automotive Engineering, Tongmyeong University, 428, Sinseon-ro, Mam-gu, Busan 608-711, Republic of Korea

ARTICLE INFO

Keywords:
High sensitive ultrasonic sensor
Chemical wood matching layer
Envelope energy
Natural gas (CH_4)

ABSTRACT

This work proposes the experimental method of using a new matching layer (chemical wood) which can measure the methane gas of the main component in natural gas from a PZT (MS-21) of the most widely using $BaTiO_3$. The experiment includes a differentiated analysis of envelope voltage, standard Gaussian distribution, acoustic pattern, and energy attenuation in a closed chamber according to an air/methane gas mixture. Experimental devices and methods were used to examine the characteristics of envelope energies via control models and transmission devices using a designed circuit, which could be fitted at resonance points of electrical signal change, frequency change, and pulse change to high sensitive ultrasonic sensors, for energy measurement regarding envelope, pattern, and attenuation. Signal analysis was used to verify the characteristics of transmission signal, voltage, shape, and frequency of the envelope which was measured factually by oscilloscope equipment. The experimental results were verified by a characteristic of acoustic energy whereby an ultrasonic sensor was diffused at minimal side energy from an λ_2 sensor, while maintaining a value of θ at a minimum of 0.3 m, 18° and maximum of 1.5 m, 15° from the envelope energy pattern characteristics. Consequently, the matching layer material of general ultrasonic sensors has a significant weakness in not transferring a receiving signal that includes strength, permeability, and directivity of acoustic energy in a gaseous medium.

1. Introduction

Ultrasonic wave sensors are a promising form of technology that have been applied to many measurement gauges such as level [1,2], concentration, and thickness [3], and a range of processes and devices including cleaning [4], welding [5], motors [6], humidifiers [7], and medical appliances across a variety of environmental and industrial fields [8,9]. Ultrasonic sensors are used with techniques which can measure variation in characteristics from acoustic energy among frequencies over 20 kHz [10]. In particular, ultrasonic technology is advantageous for its ability to miniaturize fuel measurement in automobile fields and it is still being developed as a valuable measuring instrument for examining fuel levels in gasoline as well as diesel [11] and natural gas [12]. General ultrasonic sensors have the advantage of being able to easily measure the receiving energy in a high-density medium in the order of air < liquid < solid [13]. However, it is difficult to accurately measure acoustic energy in ultrasonic waves in a diffused medium such as natural gas (CH_4) or ideal gas [14].

These problems can be solved when the composition of matching layers is examined regarding characteristics from designed PZT in ultrasonic sensors [15]. The matching layer of ultrasonic sensors is used to design a method of material use calculated by theoretical equations [16]. The acoustic energy present in ultrasonic waves is characterized by a mixture of longitudinal waves [17] and transverse waves [18], and transverse waves in a gaseous medium have a weakness in the way they extinguish the partial energies that attenuate about 1/2 of the energy from actual energies. Therefore, the matching layer, which can create longitudinal waves, has an advantage in that it can improve energy increase, noise reduction, and the transmission coefficient in a gaseous medium such as natural gas [19,20].

The ceramic material used in general ultrasonic wave sensors is a form of polycrystalline material [21]. This polycrystalline material uses the PZT, PT, PZT-complex perovskite, and $BaTiO_3$, and the PZT ceramic [22] has the widest range of applications such as vibration and acting as a filter [23], resonator [24], ignition element [25], and sensor at a reasonable price. Also, the matching layer for the acoustic performance of ultrasonic waves, uses the numerous materials according to the medium of measuring objective, and ultrasonic energy is very

* Corresponding author.
E-mail address: imsy@tu.ac.kr (S.Y. Im).

https://doi.org/10.1016/j.ultras.2018.07.009
Received 13 February 2018; Received in revised form 25 June 2018; Accepted 16 July 2018
Available online 27 July 2018
0041-624X/

important for controlling technology in methods used to amplify envelope energy [26]. The first method of amplifying acoustic energy [27] uses consolidated materials for density increase or decrease, and the second method involves input voltage being amplified compulsively in control systems, circuits [28], and algorithms [29]. In particular, the use of acoustic energy analyzes the energy's performance with trigger technology in accordance with voltage height [30], shape, phase, width and the location's envelope energy change from the receiving signal.

This work proposes the experimental method of using a new matching layer (chemical wood) which can measure the methane gas of the main component in natural gas from a PZT (MS-21) of the most widely using $BaTiO_3$. Where definition of "Chemical wood" is the epoxy which includes the chemical raw materials mixed as acetic acid, alcohol, synthetic resins, artificial wood, acetone by carbonization. Particularly, this chemical wood is a promising matching layer (material) for developing ultrasonic sensor which can measure the longitudinal wave in gas fuel area. The experiment includes a differentiated analysis of envelope voltage, standard Gaussian distribution, acoustic pattern, and energy attenuation in a closed chamber according to an air/methane gas mixture.

2. Experimental devices and methods

Fig. 1 depicts a structural diagram of the conventional and high sensitive ultrasonic sensors designed by the authors for this experiment. The conventionally designed ultrasonic sensor was bonded on the lower section base of a PZT ceramic center, and the structure was designed on a PZT face with absorbent materials used to reduce the acoustic energy transferred towards the backing section. Also, the conventional ultrasonic sensor was designed by a method of inserting an epoxy which is flexible in empty space to minimize changing properties according to residual noise, impact, and temperature change. On the structural diagram the authors outline in detail the high sensitivity ultrasonic sensor used to measure a gaseous medium. The structure of the high sensitivity ultrasonic sensor was designed to maintain balance by resonance phenomena on a sidepiece comprising a PZT ceramic and cork material. Also, the matching layer was designed to increase transmission energy by its use of a chemical wood material so that acoustic energy could only be transmitted in a gaseous medium.

The matching layer sidepiece was designed to toughen the acoustic energy transmission coefficient by bonding a cork material so that the

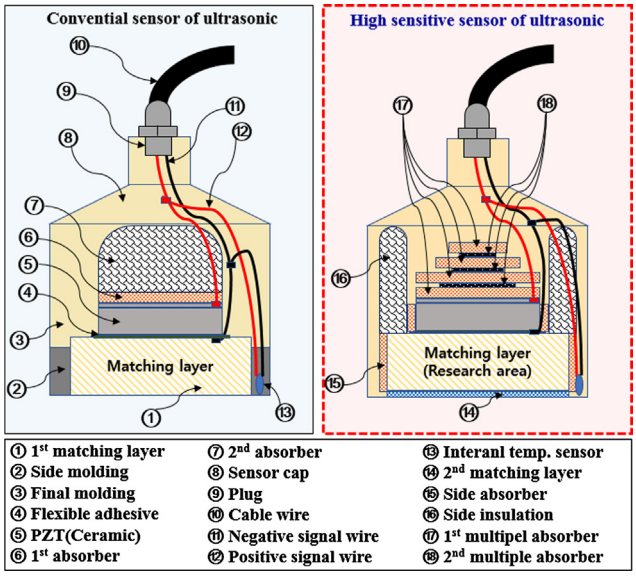

Fig. 1. Structural diagram of conventional and high sensitivity ultrasonic sensors.

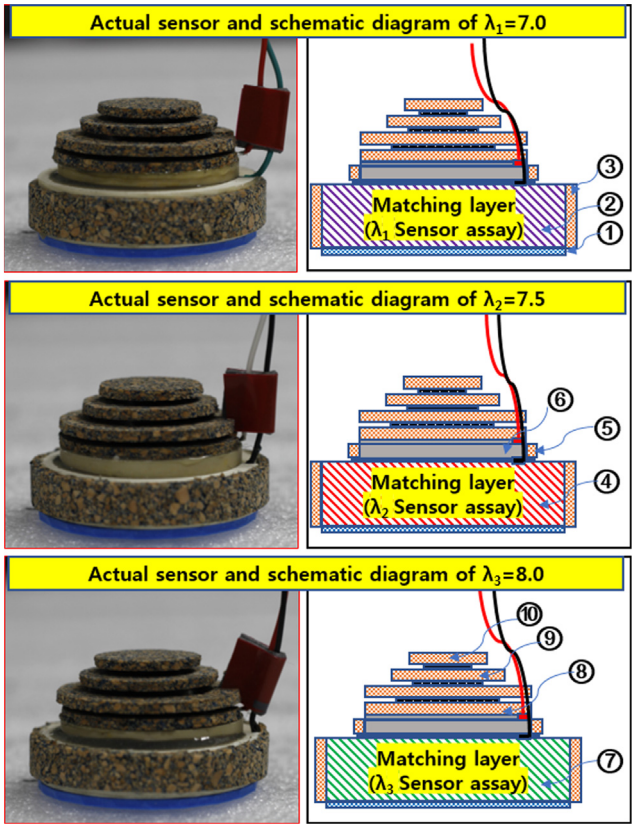

Fig. 2. Actual models of high sensitivity ultrasonic sensors for gas measurement.

ringing signal, created by self-vibrations, could be absorbed, and the face of the ultrasonic wave sensor was designed to greatly amplify the acoustic energy in a gaseous medium via its EVA (ethylene vinyl acetate) material. Additionally, the absorbent structure was designed to gradually extinguish energy towards the backing section of the conical shaped structure through its use of cork and rubber materials.

Fig. 2 depicts actual models of the high sensitivity ultrasonic sensors developed to measure the envelope energy of an air/methane gas mixture. These models can be referred to as sensor assays due to their capability of determining ultrasonic sensor performance, and may be divided into PZT ceramic, matching layer and backing layer components. Where PZT ceramic performs the role of converting electronic energy to acoustic energy, the matching layer performs a supporting role so that acoustic energy, created on the PZT ceramic face, is fitted with a methane gaseous medium and acoustic rate. The backing layer acts to absorb acoustic energy that is created on the backing face of the PZT ceramic. The authors calculated the λ (wavelength) rate of the matching layer to create the greatest envelope energy using the theoretical equation [31]:

$$\lambda = \frac{V}{f_r} \tag{2-1}$$

where V is sound velocity (430 m/s) of CH_4 fuel, and f_r is resonance frequency for the PZT ceramic. Additionally, fundamental resonance frequency of PZT ceramic is divided into 2 methodologies (minimizing and maximizing impedance frequencies) measured by impedance analyzer (4294A of Agilent Technology). MS-21 PZT ceramic used in this work has a fundamental resonance frequency encompassed minimum (46.6 kHz) and maximum (51.3 kHz). Table 1 shows the materials and specifications of the ultrasonic sensors for CH_4 gas, and Table 2 shows the acoustic properties of material inside the ultrasonic sensors for CH_4 gas.

Table 1
Materials and specifications of ultrasonic sensors for CH_4 gas.

No	Material	Specifications
①	Ethylene vinyl acetate	Ø45 * 2.0 [mm]
②	Chemical wood (λ_1 of matching layer)	Ø45 * 7.0 [mm]
③	Cork (side of matching layer)	Ø46 * 1.0 [mm]
④	Chemical wood (λ_2 of matching layer)	Ø45 * 7.5 [mm]
⑤	Cork (side of ceramic)	Ø46 * 1.0 [mm]
⑥	Piezoelectric ceramic (F_r: min. (46.6 [kHz]) and max. (51.3 [kHz]))	Ø35 * 3.0 [mm]
⑦	Chemical wood (λ_3 of matching layer)	Ø45 * 8.0 [mm]
⑧	Cork (backing 1st of ceramic)	Ø35 * 1.0 [mm]
⑨	Cork (backing 2nd of ceramic)	Ø25 * 1.0 [mm]
⑩	Cork (backing 3rd of ceramic)	Ø15 * 1.0 [mm]

Table 2
Acoustic properties of material inside ultrasonic sensor for CH_4 gas.

Material	V_L [mm/s]	Density [g/cm^3]	Z_L [MRayl]
Ethylene vinyl acetate (at 20 °C)	1.80	0.94	1.69
Chemical wood (at 20 °C)	2.84	0.65	1.85
Cork (at 20 °C)	0.50	0.24	0.12
Piezoelectric ceramic (at 20 °C)	4.72	7.95	37.5
CH_4 (at 20 °C)	0.43	0.72	0.31

Figs. 3 and 4 show the acoustic attenuation characteristics of envelope energy transferred from the transmission sensor to the receiver sensor in a gaseous medium of natural gas, by creating the conventional ultrasonic sensor and high sensitivity ultrasonic sensor. As noted above, the conventional ultrasonic sensor has an extinguishing characteristic that was not transferred in a gas layer from the transmission sensor to the receiving sensor with acoustic energy. On the other hand, the high sensitivity ultrasonic sensor transfers to the receiving sensor face a large amount of energy via an impedance characteristic that can be amplified by a matching layer (chemical wood material) of acoustic energy in a gaseous layer. These characteristics can be clearly defined as acoustic impedance by the high sensitivity ultrasonic sensor, and the authors used the following equation of energy characteristics between transmission and reflection coefficient to verify this:

$$\boldsymbol{T} = \frac{4\boldsymbol{Z}_{L,1}\boldsymbol{Z}_{L,2}}{(\boldsymbol{Z}_{L,1}+\boldsymbol{Z}_{L,2})^2} \quad \text{and} \quad \boldsymbol{R} = \frac{(\boldsymbol{Z}_{L,2}-\boldsymbol{Z}_{L,1})^2}{(\boldsymbol{Z}_{L,2}+\boldsymbol{Z}_{L,1})^2} \tag{2-2}$$

where $\boldsymbol{T}$ is the transmission coefficient which was transferred from ultrasonic wave sensor, and $\boldsymbol{R}$ is the reflection coefficient, which was returned with the envelope energy, from the transmission sensor to the receiving sensor. Also, $\boldsymbol{Z}_{L,1}$ is the acoustic impedance of the primary medium, and $\boldsymbol{Z}_{L,2}$ is the acoustic impedance of the secondary medium. $\boldsymbol{Z}_{L,3}$ and $\boldsymbol{Z}_{L,4}$ are calculated equally from Eq. (2-2).

The matching layer of the ultrasonic wave sensor is determined as the receiving performance of envelope energy from the longitudinal wave, and the longitudinal wave's energy is defined as the following equation [32]:

$$\boldsymbol{V}_L = \sqrt{\frac{\boldsymbol{E}(1-\boldsymbol{\mu})}{\boldsymbol{\rho}(1+\boldsymbol{\mu})(1-2\boldsymbol{\mu})}} \tag{2-3}$$

where $\boldsymbol{V}_L$ is the velocity of the longitudinal wave transferred by the PZT ceramic of the ultrasonic sensor, and $\boldsymbol{E}$ is defined as modulus of elasticity. Finally, ρ is the density of the matching layer's medium, and $\boldsymbol{\mu}$ is defined as "Poisson's Ratio".

Additionally, the matching layer of the ultrasonic sensor changes the direction of energy via acoustic refraction in a process that transfers longitudinal wave energy from the PZT ceramic, and these changes were calculated using "Snell's Law" (of refraction) [33].

$$\frac{\mathbf{Sin}\boldsymbol{\theta}_I}{\mathbf{Sin}\boldsymbol{\theta}_R} = \frac{\boldsymbol{V}_1}{\boldsymbol{V}_2} \tag{2-4}$$

Where $\boldsymbol{\theta}_I$ is the angle of the incident wave, $\boldsymbol{\theta}_R$ is defined as the angle of the reflected wave $\boldsymbol{V}_1$ is the velocity of the incident wave, and $\boldsymbol{\theta}_R$ is defined as the velocity of the reflected wave.

The energy that can be transferred from the methane gas layer to the

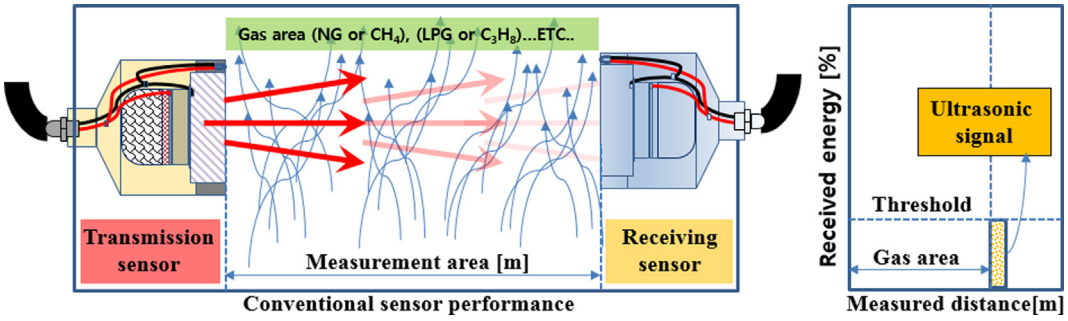

Fig. 3. Schematic diagram of characteristic with conventional ultrasonic sensor.

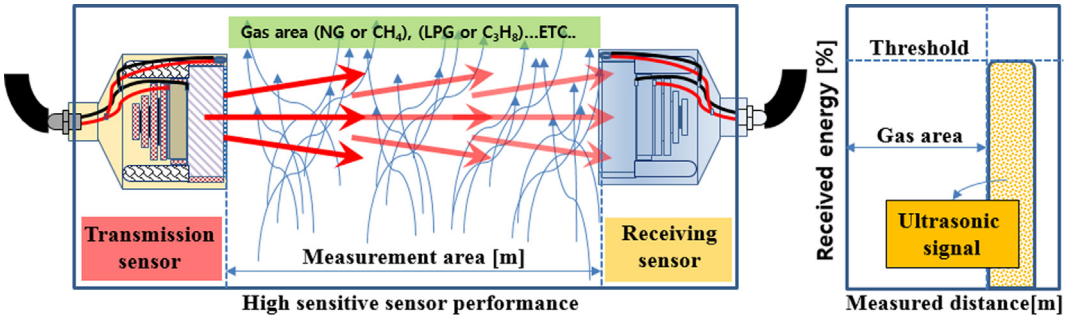

Fig. 4. Schematic diagram of characteristic with high sensitivity ultrasonic sensor.

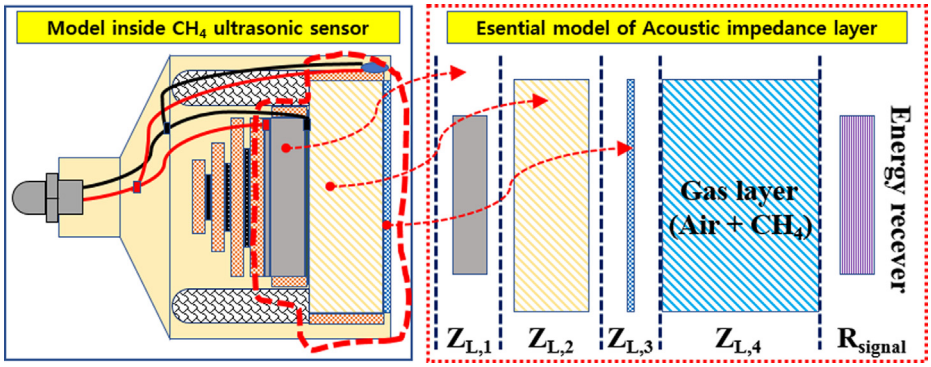

Fig. 5. Definition of acoustic impedance for each section.

PZT ceramic face can be verified by the transmission coefficient rate by acoustic impedance, and acoustic impedance is defined by the following equation [34]:

$$Z_L = \rho V \tag{2-5}$$

where is the value of acoustic impedance from the PZT ceramic to the methane medium, and ρ is defined as density from the PZT ceramic to methane medium, and V is defined as the velocity from the PZT ceramic to methane medium (seeFig. 5).

Fig. 6 depicts a schematic diagram of experimental devices and systems for envelope signal measurement from high sensitive ultrasonic wave sensors.

Experimental devices were designed in sections, with system controls, energy analysis, mechanical control, and signal analysis. The system control section was conducted by the Labview program with mass flow controllers of air, oxygen, and methane so that energy could be measured in a closed chamber. In particular, oxygen used in this experiment was controlled so as to add a specific gravity of air mass which was lacking in a closed chamber. Also, the air/methane mixture rate was calculated academically by the following equation [35,36]:

$$\lambda = \frac{F/A}{(F/A)_s} \tag{2-6}$$

where F is actual mass of methane gas and A is actual mass of air. Also, $(F/A)s$ is defined as the stoichiometric ratio or theoretical ratio of air/methane.

The energy analysis section was installed with a control module by designing a circuit which could fit the resonance point of electric signal changes, frequency changes, and pulse changes in the PZT ceramic face from the high sensitivity ultrasonic sensor. The mechanical control section was designed to analyze results changed by attenuated characteristics from envelope energy according to air/methane gas, by

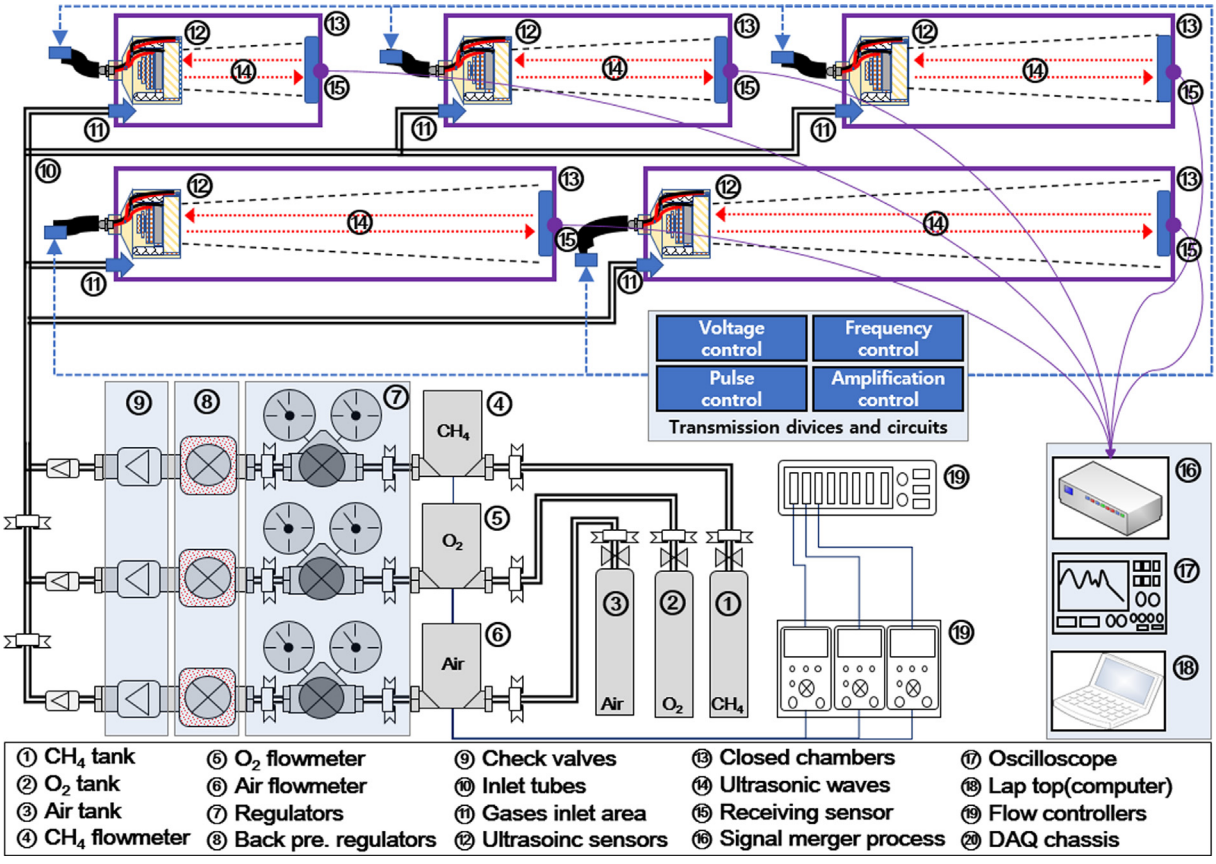

Fig. 6. Schematic diagram of experimental devices and systems for signal measurement of high sensitivity ultrasonic wave sensors.

Table 3
Specifications of experimental devices and systems.

Experimental devices	Specifications
Mass flow controller (Air)	Min. 0 to max. 5.0 [L/m]
Mass flow controller (O_2)	Min. 0 to max. 1.5 [L/m]
Mass flow controller (CH_4)	Min. 0 to max. 1.5 [L/m]
Check valves	Max. 30 [bar]
Closed vessels	∅100∗0.3[m], 0.6[m], 0.9[m], 1.2[m], 1.5[m]
Voltage controller	Min. 5 to max. 35 [V]
Frequency controller	Min. 10 to max. 300 [kHz]
Pulse controller	Width (min 3 to max. 15 [Hz]), High (min 0 to 35 [V])
Amplification controller	1 * 1, 1 * 10, 1 * 100, 1 * 1000
Regulators	100 to 20 [bar]
Oscilloscope	70 [MHz]

Table 4
Specifications of control scales for gas (Air/ CH_4 mixture) measurement.

Classifications	Specifications of control
Mass flow and voltage of Air	5.0 [L/m] and 0 to 5 [V]
Mass flow and voltage of O_2	1.5 [L/m] and 0 to 5 [V]
Mass flow and voltage of CH_4	1.5 [L/m] and 0 to 5 [V]

Table 5
Experimental conditions for measurement of high sensitivity ultrasonic wave sensors.

Properties	Experimental conditions inside closed vessels
Initial pressure	Fixed 2 [bar]
Initial temperature	296 [K]
Sensor type	λ = 7.0, 7.5, 8.0
Fuels	Air, O_2 and CH_4
Strength of voltage and current	25 [V] and 0.5 [A]
Pulse	Fixed 3 [Hz]
Resonant frequencies	λ_1 = 7.0 (61.4 [kHz]), λ_2 = 7.5 (57.3 [kHz]) and λ_3 = 8.0 (53.7 [kHz])
Sensor measurement distances	0.2 to 2.0 [m], 0.4 unit
Analysis subject	Longitudinal wave by ultrasonic transmission

being installed in closed chambers with 5 types from high sensitivity ultrasonic sensors for each model. The signal analysis section was conducted to analyze transmission and receiving characteristics of signals, voltages, shapes, and frequency from envelope energies with actual measurement. The algorithm at use in this procedure was applied to the Labview system for detailed analysis of each envelope energy from the standard Gaussian distribution. Table 3 shows the detailed

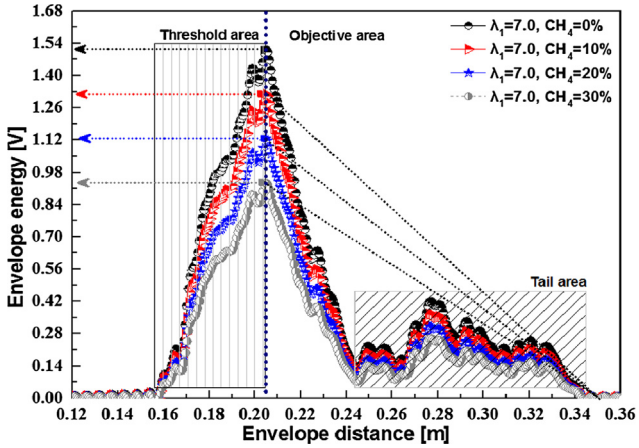

Fig. 7. (a) Result of λ_1 = 7.0, CH_4 10 to 30% with air. (b) Result of λ_2 = 7.5, CH_4 10 to 30% with air. (c) Result of λ_3 = 8.0, CH_4 10 to 30% with air.

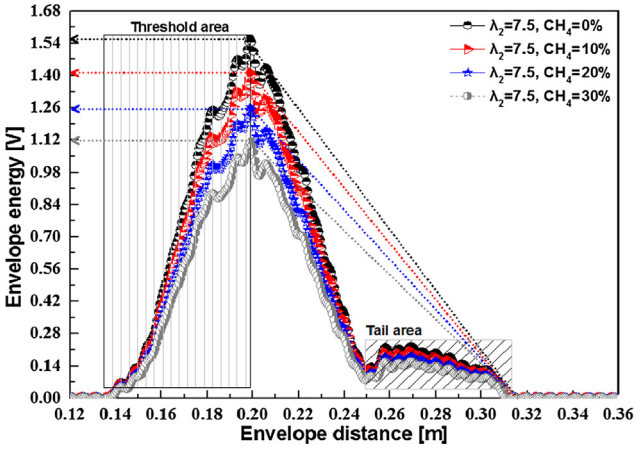

Fig. 7. (*continued*)

specifications of the experimental devices and systems and Table 4 shows the communication scales of mass flow controllers.

Table 5 shows the experimental conditions for measurement of the high sensitivity ultrasonic sensors. The experimental conditions are set at 2 bars of initial pressure so that the experiment could be conducted equally according to air/methane mixture rate. Temperature was maintained by a controller at 296 K in closed chambers which were mixed with air/methane gas. Sensors for the experiment were conducted using models designed to increase the envelope energy from matching layers (λ_1 = 7.0, λ_2 = 7.5 and λ_3 = 8.0) by Eq. (2-1), and air, oxygen, and methane gas were used as fuel. Voltage strength was controlled at 25 V, 0.5 A for each model, and pulse was fixed at 3 Hz. The distance gap between the transmission and receiving sensors was altered by 0.2 units from 0.2 m to 2.0 m, and energy was transferred equally in the PZT ceramics of each model.

From these conditions, the experiment was conducted on the application of ultrasonic waves and envelope energies in a closed chamber based on an air/methane mixture.

3. Results and discussions

Fig. 7 shows the received results of the envelope energy, which was generated by matching layers (λ_1 = 7.0, λ_2 = 7.5 and λ_3 = 8.0) inside high sensitive ultrasonic sensors, from methane 10% to 30% at 0.2 m in a closed chamber with air.

The initial voltage of received energy, which was measured from the λ_1 sensor, was verified to have increased envelope voltage at 0.16 m, and the envelope signal was changed by a characteristic created at 0.202 m with the greatest height energy from a received sensor. Also,

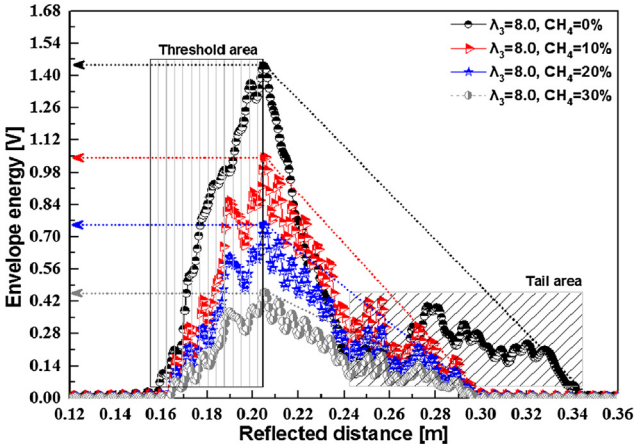

Fig. 7. (*continued*)

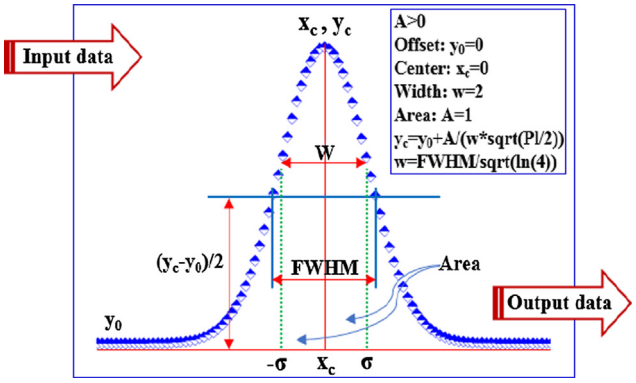

Fig. 8. A code element (algorithm) of Gaussian equation for envelope energy analysis.

the threshold result was verified as gradually attenuating the envelope signal in the order of air/methane mixture rates of CH_4 10% < 20% < 30% in a closed chamber, and the attenuated width from the mixture rate was shown to reduce energy from 1.5 V to 0.93 V according to air/methane mixture rates. The tail section of the envelope signal was analyzed as having a characteristic created with length 0.1 m and noise signal from 0.24 m to 0.34 m, and the tail characteristics were verified to proportionally extinguish the attenuated energy at the area of maximum voltage.

Consequentially, the energy characteristics were not transferred smoothly in the air/methane mixture layer by resonance energy which was designed with a smaller ratio of matching layer volume rate than the PZT ceramic's volume rate inside the λ_1 sensor, and the increased characteristics of acoustic energy was notable in that an unstable envelope signal was changed in the tail area with the highest missed energy transferred in the air/methane mixture layer.

The initial voltage of received energy, measured from a λ_2 sensor, was verified to quickly increase the envelope voltage at 0.14 m by the λ_2 sensor then the λ_1 sensor, and the envelope signal was verified by a differentiated characteristic created at 0.2 m with the most height energy from a received sensor. Also, the threshold result of the λ_2 sensor was verified to gradually attenuate the envelope signal -in a closed chamber, and the attenuated width from the mixture rate of the λ_2 sensor could be verified as reducing energy from 1.5 V to 1.11 V according to air/methane mixture rates. The tail section of the envelope signal of the λ_2 sensor was verified as having the most improved characteristics, which was created with length 0.06 m, without any noise signal from 0.25 m to 0.31 m, and the tail characteristics of the λ_2 sensor was verified as having the sharpest signal at an envelope distance between 0.13 m and 0.2 m. However, it was shown that threshold points were extinguished proportionally by attenuated energy at maximum voltages.

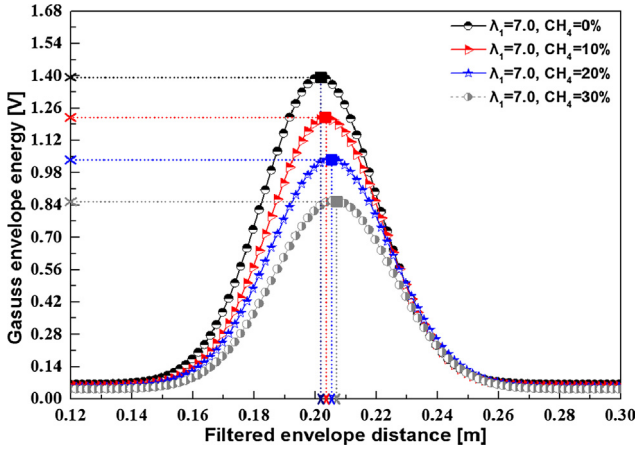

Fig. 9. (a) Filtered result of gas envelope energy at λ_1 = 7.0 with CH_4 10 to 30%. (b) Filtered result of gas envelope energy at λ_2 = 7.5 with CH_4 10 to 30%. (c) Filtered result of gas envelope energy at λ_3 = 8.0 with CH_4 10 to 30%.

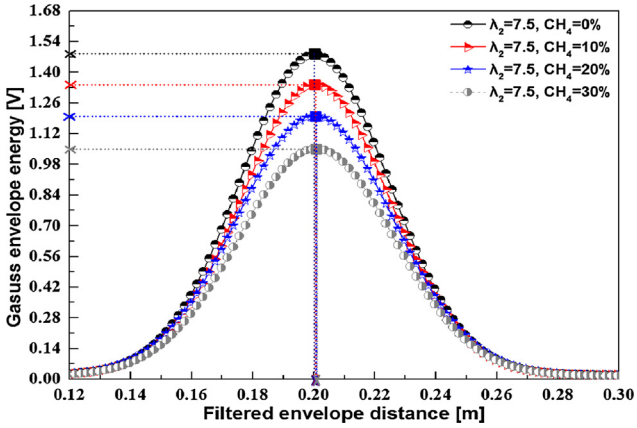

Fig. 9. (*continued*)

Consequentially, the energy characteristics were transferred smoothly in the air/methane mixture layer by resonance energy which was designed as the most suitable ratio for the matching layer's volume rate than the PZT ceramic's volume rate inside the λ_2 sensor, and the increased characteristics of acoustic energy could be predictable in that a stable envelope signal was changed in the tail area with the least missed energy, which was transferred in the air/methane mixture layer by the λ_2 sensor.

The initial voltage of received energy, measured by a λ_3 sensor, was verified as having an equal result to the λ_1 sensor and the λ_2 sensor of increased envelope signal. Maximum and minimum points could be verified as largely attenuating the envelope signal of the value measured by the λ_3 sensor then the λ_1 sensor and the λ_2 sensor for envelope voltages. The tail section of the envelope signal of the λ_3 sensor was verified to change the overlapping envelope characteristics in terms of unstable signal, untrustworthy energy, and abnormal voltage.

Consequentially, energy characteristics were transferred aberrantly in the air/methane mixture layer by resonance energy which was designed as the most unsuitable ratio of relationship between the matching layer volume rate and the PZT ceramic volume rate inside the λ_3 sensor. The increased characteristics of acoustic energy could be predictable in that heteroclite envelope signal is changed in the tail area with the highest missed energy transferred in the air/methane mixture layer by the λ_3 sensor.

Synthetically, this experiment is notable in that the conventional ultrasonic sensor has a characteristic which was extinguished in the air/

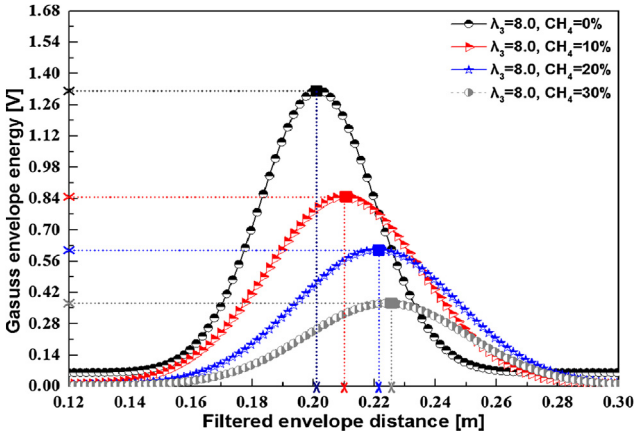

Fig. 9. (*continued*)

Table 6
Analyzed data through standard Gaussian distribution of λ_1 = 7.0.

Classification	λ_1=7.0, CH_4=0%	λ_1=7.0, CH_4=10%	λ_1=7.0, CH_4=20%	λ_1=7.0, CH_4=30%	Average value [%]
y0 [V]	0.06494	0.05652	0.05178	0.04288	5.4%
Xc [m]	0.20212	0.20423	0.20614	0.20817	20.5%
W [m]	0.0374	0.03741	0.03722	0.03722	3.7%
A [m^2]	0.06234	0.05438	0.04606	0.03815	5.0%
Sigma [--]	0.0187	0.0187	0.01861	0.01861	1.9%
FWHM [m]	0.04404	0.04404	0.04383	0.04383	4.4%
Height [m]	1.32992	1.15996	0.98734	0.81773	107.4%

Table 7
Analyzed data through standard Gaussian distribution of λ_2 = 7.5.

Classification	λ_2=7.5, CH_4=0%	λ_2=7.5, CH_4=10%	λ_2=7.5, CH_4=20%	λ_2=7.5, CH_4=30%	Average value [%]
y0 [V]	0.02098	0.01901	0.01849	0.01621	1.9%
Xc [m]	0.19857	0.19857	0.19857	0.19857	19.9%
W [m]	0.04855	0.04856	0.04847	0.04847	4.9%
A [m^2]	0.08894	0.08066	0.07181	0.06295	7.6%
Sigma [--]	0.02428	0.02428	0.02423	0.02423	2.4%
FWHM [m]	0.05717	0.05717	0.05707	0.05707	5.7%
Height [m]	1.46154	1.3255	1.18214	1.03624	125.1%

Table 8
Analyzed data through standard Gaussian distribution of λ_3 = 8.0.

Classification	λ_3=8.0, CH_4=0%	λ_3=8.0, CH_4=10%	λ_3=8.0, CH_4=20%	λ_3=8.0, CH_4=30%	Average value [%]
y0 [V]	0.06175	0.01008	0.00803	0.00489	2.1%
Xc [m]	0.20149	0.21017	0.21015	0.21015	21.5%
W [m]	0.0374	0.05042	0.0503	0.0503	4.7%
A [m^2]	0.0592	0.05299	0.03798	0.02313	4.3%
Sigma [--]	0.0187	0.02521	0.02515	0.02515	2.4%
FWHM [m]	0.04403	0.05937	0.05922	0.05922	5.5%
Height [m]	1.26306	0.83844	0.60243	0.36693	76.8%

methane mixture layer in a closed chamber by acoustic energy from the PZT ceramic. However, the high sensitivity ultrasonic sensor designed via matching layer (chemical wood and EVA) is notable in that acoustic energy could penetrate the air/methane mixture layer because of increase in acoustic strength.

Fig. 8 shows a component (algorithm) of Gaussian distribution which is most widely used for analyzing a method regarding probability distribution according to continuous signal changes. A graph is generated to process the input data so as to transfer envelope energy from actual signal, and filtered data from a Gaussian algorithm transferred towards the output area for analysis.

The authors could utilize this as differentiated data filtered by the Gaussian algorithm of actual envelope signals, and ultrasonic envelope energy could be calculated by the following equation;

$$y = y_0 + \frac{A}{w\sqrt{\pi/2}} e^{-2\frac{(x-x_c)^2}{w^2}} \quad (3\text{-}1)$$

where y_0 is the changed value of the envelope energy received from the ultrasonic wave sensor, and A is defined as the maximum value of a normal distribution. Also, w is the value (width) of the standard deviation, and x is defined as the center or average value. ***FWHM*** is described as a resolution of full width at half-maximum.

Fig. 9. shows the differentiated results of filtered envelope energy by standard Gaussian distribution, applied to the algorithm source of the analyzed data according to the air/methane mixture rate from Fig. 7.

The Gaussian values of received energy, which was changed from 0% to 30% methane, were verified to calculate the envelope energy data which was extinguished with stable signal and clear graph from the λ_1 sensor. The center (x_c) of the envelope energy was visualized to change the data in the order of 0% (0.202 m) < 10% (0.204 m) < 20% (0.206 m) < 30% (0.208 m) methane, and the voltages of envelope energy were verified to proportionally attenuate the signal with characteristics delayed at the center (x_c). However, the standard Gaussian distribution values, filtered by the λ_2 sensor data, displayed no attenuation at peak points of the envelope energy, and the center (x_c) of the envelope energy was verified as maintaining stable characteristics. The standard Gaussian distribution values, filtered by the λ_3 sensor data, was verified to have the greatest influence on peaked value and changed value at the center (x_c) of the envelope signal.

These characteristics were analyzed by differentiated results of the filtered element from the standard Gaussian distribution in Table 6, Table 7 and Table 8, and the filtered data was utilized for detailed analysis with results calculated from average values.

y_0 (initial voltage) was verified to have the most stable characteristics created in the order of λ_1 (5.4%) > λ_3 (2.1%) > λ_2 (1.9%). Also, x_c (center) exhibited the most stable result which was united at λ_2 = 7.5 of the envelope center in the order of λ_3 (21.5%) > λ_1 (20.5%) > λ_2 (19.9%). The w (envelope energy width) results had the widest signal at λ_2 = 7.5 in the order of λ_2 (4.9%) > λ_3 (4.7%) > λ_1 (3.7%). Also, A (energy area) resulted in the most widely distributed area with an average of 7.6% for the λ_2 model then 2 models in the order of λ_2 (7.6%) > λ_1 (5.0%) > λ_3 (4.3%). Additionally, σ (energy

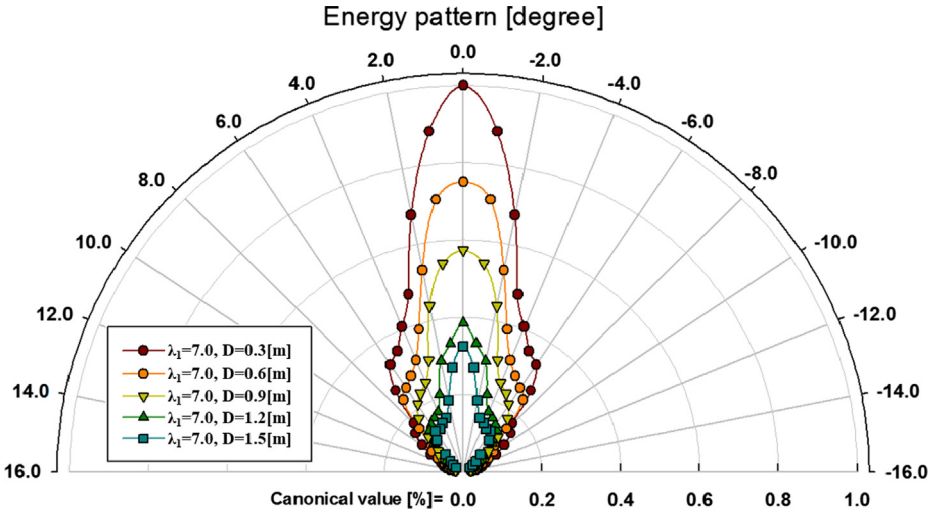

Fig. 10. (a) Energy pattern at $\lambda_1 = 7.0$ in the atmosphere. (b) Energy pattern at $\lambda_2 = 7.5$ in the atmosphere. (c) Energy pattern at $\lambda_3 = 8.0$ in the atmosphere.

sum) was verified as having equal energy for each model, and ***FWHM*** (full width at half maximum) created the most increased energy at an average of 125.1% at $\lambda_2 = 7.5$ model.

Consequentially, the characteristics of all of the section elements by standard Gaussian distribution were verified to create influential energy at $\lambda_2 = 7.5$, and the characteristics of the matching layer are notable in that the received signal, which includes envelope energy with a longitudinal wave in the air/methane mixture layer, were increased.

Fig. 10 shows the results of energy patterns analyzed experimentally regarding acoustic diffusion from the high sensitivity ultrasonic sensors. The x-axis shows the energy pattern defined as canonical value (1%) of measured energy by transmission of sensors, and the y-axis represents the energy value measured in empty space with reflectors in closed chambers from 0.3 m to 1.5 m.

The energy patterns of the λ_1 sensor were diffused with acoustic energy which was spread towards the sidepiece at minimum 11° and maximum 16° at 1.5 m. Also, the directivity of the acoustic energy was verified to reduce the envelope area according to measuring distances, and the pattern attenuation width was visualized to create an inconstant signal between 1.2 m and 1.5 m from the λ_1 sensor. The dispersion of energy displayed changed characteristics at the ringing signal area below 0.3% by the resonance frequency of 61.4 kHz from the λ_1 sensor, and the concentration of energy changed with the directivity and diffusion at the area between 0.2% and 1% from the λ_1 sensor.

These characteristics, by the directivity and diffusion of acoustic energy from the λ_1 sensor, were changed into side energy as 1/3 of acoustic wave which was created from a ringing signal then acoustic energy was created from a resonance wave. Also, the directivity of energy is notable in that the envelope signal had a negative influence on partially attenuating an ideal energy from the sidepiece.

The energy patterns of the λ_2 sensor were diffused by the lowest sidepiece signal with acoustic energy at minimum 15° and maximum 18° at 0.3 m. Also, the directivity of the acoustic energy was verified to widely diffuse the highest signal of the envelope area according to measuring distances, and the pattern attenuation width was visualized to proportionally change the most stable signal between 0.3 m and 1.5 m from the λ_2 sensor. The dispersion of energy was visualized by dead zone characteristics at the ringing signal area below 0.17% by the resonance frequency 57.3 kHz from the λ_2 sensor, and the concentration of energy was verified to change the ideal energy with the widest diffusion of directivity at the area between 0.4% and 1% from the λ_2 sensor.

These characteristics, by the directivity and diffusion of acoustic energy from the λ_2 sensor, were notable in that acoustic energy was not missed from the PZT ceramic to the receiving sensor of the transmission coefficient, created by the λ_2 matching layer (chemical wood).

The energy patterns of the λ_3 sensor were verified to have a missed characteristic of acoustic energy diffused from the highest side signal at

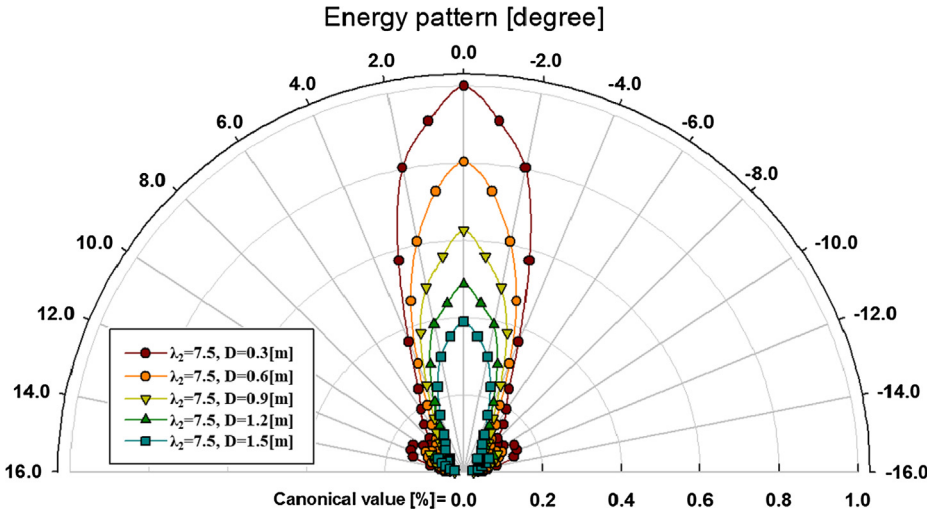

Fig. 10. (*continued*)

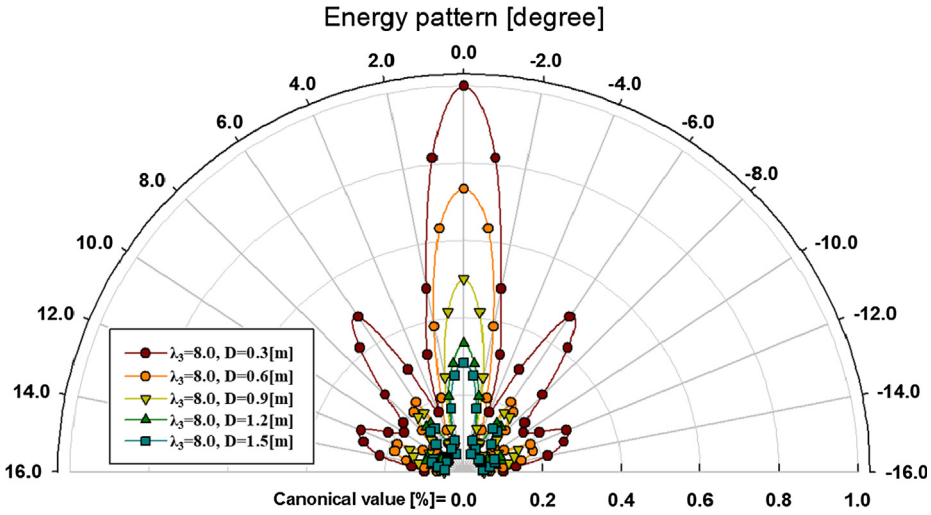

Fig. 10. (*continued*)

minimum 15° and maximum 19° at 0.3 m. Also, the directivity of the acoustic energy was verified to have an unstable characteristic which was diffused narrowly at an envelope area according to measuring distances, and the energy loss was changed into the sharply altered characteristics from 0.3 m to 1.5 m from the λ_3 sensor. Dispersion of energy was shown to be a problem which causes an inability to measure the envelope signal at a ringing signal 0.45% below the resonance frequency of 53.7 kHz from the λ_3 sensor, and the concentration of energy was verified to change the ideal energy with the least diffusion of directivity at an area between 0.5% and 1% from the λ_3 sensor.

These characteristics, by the directivity and diffusion of acoustic energy from the λ_3 sensor, were notable in that the matching layer was diffused irregularly from the PZT ceramic face to the reflector, and the envelope signal was notable in that the transmission coefficient was missed in empty space from the λ_3 sensor.

Synthetically, this experiment is notable in that energy patterns from high sensitive ultrasonic sensors were visualized by distributed characteristics such as energy shapes, diffusion, and directivity, and the concentration of envelope energy was predictable in that the λ_2 sensor, made out of chemical wood and EVA material, was suitable for measurement in an air/methane mixture layer due to high signals from such elements as acoustic energies, envelope widths, signals voltages and envelope shapes.

Fig. 11 shows the results of reception sensitivity according to air/methane mixture rate by installing the high sensitive ultrasonic sensor in a chamber, and this result was analyzed as changing the attenuation characteristics from minimum 0.2 m to maximum 2.0 m in measuring distance, including the dead zone area by PZT vibration. The x-axis of the graph represents the measured distance of envelope energy accepted from receiving sensors, and the y-axis the attenuation values of received energy according to distance change between transmission and reception sensors.

The maximum values of received energy from the methane gas mixture (0%) were measured at 0.2 m with voltage signals in the order of λ_2 (1.55 V) > λ_1 (1.51 V) > λ_3 (1.33 V), and the envelope signals were detected in the order of λ_2 (2.0 m) > λ_1 (1.8 m) > λ_3 (1.4 m). Also, the average values from 0.2 m to 2.0 m were verified to increase 10% of energy performance at the λ_2 sensor then λ_1 and λ_3 sensors in the order of λ_2 (1.06 V) > λ_1 (0.95 V) > λ_3 (0.80 V), while the λ_2 sensor was measured to have the most increased voltages of energy value (10%) then the λ_1 and λ_3 sensors.

These characteristics of sensors from the distance changes were notable in that specific gravity of fuel with reliable energy characteristics could be measured, and this experiment is notable in that acoustic energies in an air/methane mixture layer were penetrated by models such as the λ_2 sensor which was designed to fit the volume rate of PZT ceramic and a matching layer.

The value of received energy by the methane gas mixture rate (10%, 20% and 20%) in air was verified to maintain the highest voltage at the λ_2 sensor such as. The average values display results measured in the order of λ_2 (10% = 0.2 m, 20% = 1.6 m, 30% = 1.4 m) > λ_1

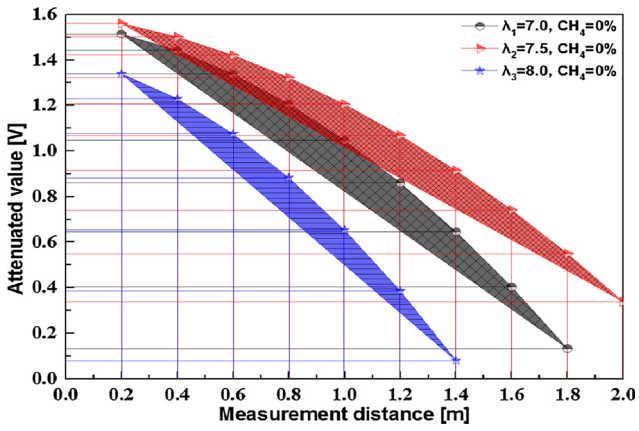

Fig. 11. (a) Reception sensitivity of air/methane mixture rate 0%. (b) Reception sensitivity of air/methane mixture rate 10%. (c) Reception sensitivity of air/methane mixture rate 20%. (d) Reception sensitivity of air/methane mixture rate 30%.

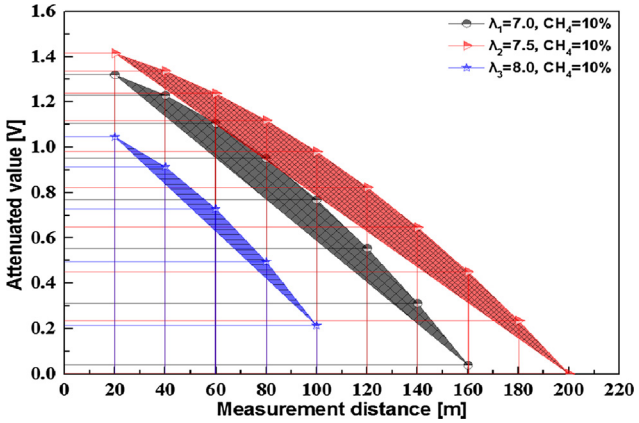

Fig. 11. (*continued*)

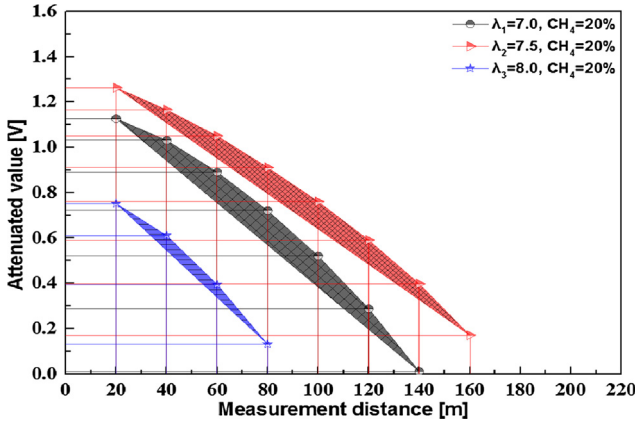

Fig. 11. (*continued*)

(10% = 1.6 m, 20% = 1.4 m, 30% = 1.0 m) > λ_3 (10% = 0.1 m, 20% = 0.8 m, 30% = 0.6 m).

These characteristics are notable in that a stable envelope signal was measured accurately because of EVA material which can amplify the penetrability energy.

Synthetically, because the general matching layer is designed to not fit the transmission coefficient between PZT ceramic and matching layer mediums with acoustic impedance (), the conventional ultrasonic sensor could not be measured. However, the materials of chemical wood and EVA are notable in that the acoustic impedance value was designed suitably for measurement in an air/methane mixture layer in the order of $\lambda_2 > \lambda_1 > \lambda_3$.

4. Conclusion

From the experimental results of the application of ultrasonic waves and envelope energies in a closed chamber based on an air/methane mixture, the following conclusions were obtained:

The energy characteristics were transferred smoothly in the air/methane mixture layer by resonance energy which was designed as having the most suitable ratio of relationship between the matching layer volume rate and the PZT ceramic volume rate inside the λ_2 sensor, and the increased characteristics of acoustic energy could be predictable in that a stable envelope signal was changed at the tail area with the least missed energy transferred in the air/methane mixture layer from the λ_2 sensor. The characteristics of all of the section elements by standard Gaussian distribution were verified to create influential energy at $\lambda_2 = 7.5$, and the characteristics of the matching layer are notable in that the received signal, which includes longitudinal wave envelope energy in the air/methane mixture layer, was increased. Furthermore, this experiment is notable in that energy patterns from high sensitive ultrasonic sensors were visualized by distributed characteristics such as energy shapes, diffusion, and directivity, and the concentration of envelope energy is predictable in that the λ_2 sensor, made with chemical wood and EVA material, is suitable for measurement in an air/methane mixture layer due to high signals from such elements as acoustic energies, envelope widths, signals voltages and envelope shapes. Synthetically, because the general matching layer is designed to not fit the transmission coefficient between PZT ceramic and matching layer mediums with acoustic impedance (), the conventional ultrasonic sensor could not be measured. However, the materials of chemical wood and EVA are notable in that acoustic impedance value was designed suitably for measurement in an air/methane mixture layer in the order of $\lambda_2 > \lambda_1 > \lambda_3$.

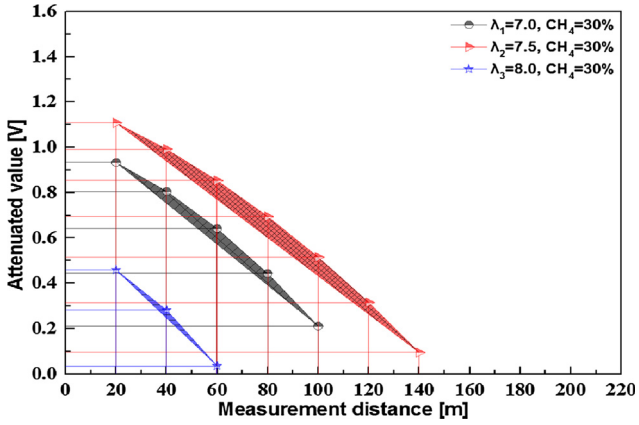

Fig. 11. (*continued*)

Acknowledgements

This research was supported by the Basic Science Research Program through the National Research Foundation of Korea (NRF) funded by the "Ministry of Education (NRF-2017R1D1A1B03031156)" and by the "Tongmyong University Research Grants" 2018(2018F019).

References

[1] Michael J. Vellekoop, Acoustic wave sensors and their technology, Ultrasonics 36 (1-5) (1998) 7–14.
[2] V.E. Sakharov, et al., Liquid level sensor using ultrasonic Lamb waves, Ultrasonics 41 (4) (2003) 319–322.
[3] Ye Lu, et al., "Quantitative assessment of through-thickness crack size based on Lamb wave scattering in aluminium plates, Ndt & E Int. 41 (1) (2008) 59–68.
[4] Hao Xu, et al., Application of ultrasonic wave to clean the surface of the TiO_2 nanotubes prepared by the electrochemical anodization, Appl. Surf. Sci. 257 (20) (2011) 8478–8480.
[5] G. Harman John Albers The ultrasonic welding mechanism as applied to aluminum- and gold-wire bonding in microelectronics IEEE Trans. Parts, Hybrids, Packaging 13.4 (1977): 406-412.
[6] Nesbitt W. Hagood, Andrew J. McFarland, Modeling of a piezoelectric rotary ultrasonic motor, IEEE Trans. Ultrasonics, Ferroelectrics, Freq. Control 42 (2) (1995) 210–224.
[7] Durley III, A. Benton, Ultrasonic humidifiers, atomizers and the like, U.S. Patent No. 4,085,893. 25 Apr. 1978.
[8] Rabiner, A. Robert, A. Bradley, Hare, Ultrasonic medical device for tissue remodeling, U.S. Patent No. 6,695,781. 24 Feb. 2004.
[9] Kevin Ashley, Ultrasonic extraction and field-portable anodic stripping voltammetry of lead from environmental samples, Electroanalysis 7 (12) (1995) 1189–1192.
[10] J. Cheeke, N. Daunsid, Fundamentals and Applications of Ultrasonic Waves, CRC press, 2016.
[11] Jaqua, W. Vance, Ultrasonic check valve and diesel fuel injector, U.S. Patent No. 4, 389,999. 28 Jun. 1983.
[12] Marco Dell'Isola, Mauro Cannizzo, Matteo Diritti, Measurement of high-pressure natural gas flow using ultrasonic flowmeters, Measurement 20 (2) (1997) 75–89.
[13] J.P. Reckless, et al., High-density and low-density lipoproteins and prevalence of vascular disease in diabetes mellitus, Br. Med. J. 1 (6117) (1978) 883–886.
[14] G.J. Prangsma, A.H. Alberga, J.J.M. Beenakker, Ultrasonic determination of the volume viscosity of N2, CO, CH4 and CD4 between 77 and 300 K, Physica 64 (2) (1973) 278–288.
[15] Takeshi Inoue, Masaya Ohta, Sadayuki Takahashi, Design of ultrasonic transducers with multiple acoustic matching layers for medical application, IEEE Trans. Ultrasonics, Ferroelectrics, Freq. Control 34 (1) (1987) 8–16.
[16] Kelly, S.P., G. Hayward, T.E. Gomez, An air-coupled ultrasonic matching layer employing half wavelength cavity resonance, Ultrasonics Symposium, 2001 IEEE, vol. 2. IEEE, 2001.
[17] R.J. Hudgell, H. Seed, Ultrasonic longitudinal wave examination of austenitic welds, Br. J. Non-Destructive Testing 22 (2) (1980) 78–85.
[18] Aleksander Pilarski, Joseph L. Rose, A transverse-wave ultrasonic oblique-incidence technique for interfacial weakness detection in adhesive bonds, J. Appl. Phys. 63 (2) (1988) 300–307.
[19] D.L. Folds, C.D. Loggins, Transmission and reflection of ultrasonic waves in layered media, J. Acoust. Soc. Am. 62 (5) (1977) 1102–1109.
[20] Borenstein, Johann, Yoram Koren, Noise rejection for ultrasonic sensors in mobile robot applications, in: Proceedings International Conference on IEEE Robotics and Automation, IEEE 1992, 1992.
[21] D.A. Berlincourt, C. Cmolik, H. Jaffe, Piezoelectric properties of polycrystalline lead titanate zirconate compositions, in: Proceedings of the IRE, vol. 48.2, 1960, pp. 220–229.
[22] Kaoru Yamashita, et al., Arrayed ultrasonic microsensors with high directivity for in-air use using PZT thin film on silicon diaphragms, Sens. Actuat. A: Phys. 97 (2002) 302–307.
[23] Davis, Scott Judson, Dan Michael Hausermann, Ultrasonic filter regenerating

apparatus and method, U.S. Patent No. 6,251,294. 26 Jun. 2001.
[24] J.G. Miller, D.I. Bolef, Sensitivity enhancement by the use of acoustic resonators in cw ultrasonic spectroscopy, J. Appl. Phys. 39 (10) (1968) 4589–4593.
[25] Ruiping Wang, et al., Piezoelectric properties of spark-plasma-sintered (Na0.5K0.5) NbO_3–$PbTiO_3$ ceramics, Jpn. J. Appl. Phys. 41 (11S) (2002) 7119.
[26] Y.P. Huang, et al., Envelope pulsed ultrasonic distance measurement system based upon amplitude modulation and phase modulation, Rev. Sci. Inst. 78 (6) (2007) 065103.
[27] Ehlert, Thomas, et al., Methods for producing ultrasonic waveguides having improved amplification, U.S. Patent Application No. 11/301,137.
[28] F.-J. Lin, L.-C. Kuo, Driving circuit for ultrasonic motor servo drive with variable-structure adaptive model-following control, IEE Proc.-Electric Power Appl. 144 (3) (1997) 199–206.
[29] L.J. Augustine, J. Andersen, An algorithm for the design of transformerless broadband equalizers of ultrasonic transducers, J. Acoust. Soc. Am. 66 (3) (1979) 629–635.
[30] Yoshiyuki Asakura, et al., Effects of ultrasonic frequency and liquid height on sonochemical efficiency of large-scale sonochemical reactors, Ultrason. Sonochem. 15 (3) (2008) 244–250.
[31] L.E. Hargrove, Effects of ultrasonic waves on Gaussian light beams with diameter comparable to ultrasonic wavelength, J. Acoust. Soc. Am. 43 (4) (1968) 847–851.
[32] Hsueh-Chang Wu, et al., Monitoring the degradation process of biopolymers by ultrasonic longitudinal wave pulse-echo technique, Biomaterials 24 (22) (2003) 3871–3876.
[33] Bernard Hosten, Reflection and transmission of acoustic plane waves on an immersed orthotropic and viscoelastic solid layer, J. Acoust. Soc. Am. 89 (6) (1991) 2745–2752.
[34] Tone, Masayuki, Tsutomu Yano, Koetsu Saito, Piezoelectric ultrasonic transducers having acoustic impedance-matching layers, U.S. Patent No. 4,523,122. 11 Jun. 1985.
[35] Kwonse Kim, Dooseuk Choi, Research on the reaction progress of thermodynamic combustion based on arc and jet plasma energies using experimental and analytical methods, J. Mech. Sci. Technol. 32 (4) (2018) 1869–1878.
[36] Chan-Wei Wu, et al., The influence of air–fuel ratio on engine performance and pollutant emission of an SI engine using ethanol–gasoline-blended fuels, Atmosp. Environ. 38.40 (2004) 7093–7100.